THE JOURNAL OF CHEMICAL PHYSICS **134**, 044702 (2011)
http://link.aip.org/link/JCPSA6/v134/i4/p044702/s1

Reversible uptake of water on NaCl nanoparticles at relative humidity below deliquescence point observed by noncontact environmental atomic force microscopy

Derek A. Bruzewicz,[1,2] Antonio Checco,[1,a)] Benjamin M. Ocko,[1] Ernie R. Lewis,[2] Robert L. McGraw,[2] and Stephen E. Schwartz[2]
[1]*Condensed Matter Physics and Materials Science Department, Brookhaven National Laboratory, Building 510-B, Upton, New York 11973, USA*
[2]*Atmospheric Sciences Division, Environmental Sciences Department, Brookhaven National Laboratory, Building 815-E, Upton, NY 11973, USA*

(Received 9 July 2010; accepted 12 November 2010; published online 24 January 2011)

The behavior of NaCl nanoparticles as a function of relative humidity (RH) has been characterized using non-contact environmental atomic force microscopy (e-AFM) to measure the heights of particles deposited on a prepared hydrophobic surface. Cubic NaCl nanoparticles with sides of 35 and 80 nm were found to take up water reversibly with increasing RH well below the bulk deliquescence relative humidity (DRH) of 75% at 23°C, and to form a liquid-like surface layer of thickness 2 to 5 nm, with measurable uptake (>2 nm increase in particle height) beginning at 70% RH. The maximum thickness of the layer increased with increasing RH and increasing particle size over the range studied. The liquid-like behavior of the layer was indicated by a reversible rounding at the upper surface of the particles, fit to a parabolic cross-section, where the ratio of particle height to maximum radius of curvature increases from zero (flat top) at 68% RH to 0.7 ± 0.3 at 74% RH. These observations, which are consistent with a reorganization of mass on the solid NaCl nanocrystal at RH below the DRH, suggest that the deliquescence of NaCl nanoparticles is more complex than an abrupt first-order phase transition. The height measurements are consistent with a phenomenological model that assumes favorable contributions to the free energy of formation of a liquid layer on solid NaCl due both to van der Waals interactions, which depend partly upon the Hamaker constant, A_{film}, of the interaction between the thin liquid film and the solid NaCl, and to a longer-range electrostatic interaction over a characteristic length of persistence, ξ; the best fit to the data corresponded to $A_{film} = 1\ kT$ and $\xi = 2.33$ nm. © *2011 American Institute of Physics*. [doi:10.1063/1.3524195]

I. INTRODUCTION

Deliquescence—the phase transition from a solid to a solution that occurs when, at a given temperature, the relative humidity (RH) increases to the deliquescence RH (DRH)—has long been studied in the fields of physical chemistry,[1,2] condensed matter physics,[3–5] nanoscience,[6–9] and atmospheric science.[10–15] For a given pure solute, the value of the DRH depends weakly on temperature,[16–18] and the phase transition of the bulk material, which exhibits negligible surface effects, is generally considered first-order.[1] Recent investigations, however, have demonstrated that uptake of water on a dry solute can occur at RH less than the DRH, both as monolayers of pure water[5] and as bulk-like layers of solution around a solid core.[15] The physical interactions that drive the uptake of water below the DRH remain unknown, and different results for the maximum thickness of predeliquescent liquid layers for the minimum RH at which the uptake first occurs have been reported.[6–9,15] Such uptake could be important for atmospheric chemistry by providing a liquid phase for chemical reactions, such as those responsible for depletion of ozone in the lower troposphere at high latitudes in the spring.[19,20]

Uptake of water by inorganic solutes at RH below the DRH has been documented in several prior studies. Surface x-ray diffraction experiments by Arsic *et al.* established the presence of layers of water less than 1-nm thick on bulk NaCl surfaces at RH as low as 45%.[21] Early experiments by Salmeron and colleagues used contact-mode AFM to confirm the presence of water on NaCl crystals at 40% RH by showing that steps and other topological features migrate over time as ions dissolve and diffuse.[13,14] Investigations of water uptake on crystalline NaCl by Peters *et al.* using Fourier-transform infrared spectroscopy (FTIR) demonstrated reversible adsorption of water between ~50% and 70% RH,[22] but the FTIR method provided little information about layers of water thicker than approximately 4 monolayers (i.e., at RH above ~70%).

Phase transitions of soluble inorganic salts have been studied by a variety of techniques, some of which require that the sample be deposited on an insoluble substrate prior to measurement. The use of an electrodynamic balance, which does not require such a substrate, is a very powerful method to study levitated single particles and supersaturated solution drops at RH ranging from near 0% to well above the DRH of many common salts.[10–12] This technique revealed an apparently sharp, first-order transition from a crystal to a drop of solution for pure NaCl.[10] This phase transition was found to be

a)Electronic mail: checco@bnl.gov

kinetically irreversible: upon reducing the RH of the environment around a deliquesced NaCl particle to a value below the DRH, the particle remained a (supersaturated) solution until a nucleation event occurred at the so-called efflorescence RH (~45% at room temperature), at which point the water was abruptly expelled and the particle returned to the solid state. An individual particle could be repeatedly cycled through the deliquescence/efflorescence phase transition.[10–12]

Spectroscopic methods, which also need not require an underlying substrate,[23,24] have been used to measure the thickness of an aqueous layer on solid particles flowing in moist air. These techniques, and also differential mobility analysis,[25,26] can detect changes of a few nanometers in the radius of particles with diameter less than 1 μm by examining ensembles of particles and extracting an average effect. In general, these methods have difficulty revealing any subtle changes in topology, although Mifflin *et al.* have used mobility analysis to infer morphology indirectly in work that attributes variable rates of water uptake in ammonium bisulfate particles to differences in their morphology.[27]

Scanning probe techniques allow determination of the size and shape of individual particles smaller than ~500 nm across mounted on a substrate. Using scanning polarization force microscopy (SPFM) with an AFM tip held at an oscillating electrical potential relative to the sample, Arima *et al.*[9] reported that KBr particles initially less than 30 nm in height at 20% RH increased by more than 15 nm in height at 71% RH (i.e., well below the bulk deliquescence point of near 80% at room temperature[28]). This technique is particularly sensitive to the electrostatic forces between the tip and the polarized sample, and therefore to the concentration of dissolved ions near the liquid-air interface. Because the force between the sample and probe tip is sensitive to changes in both the height and the polarizability of the sample, Arima *et al.* noted that apparent increases in height are likely due to both adsorption of water onto the sample and solvation of ions in the liquid layer. The technique is somewhat insensitive to changes in the morphology of particles because the probe scans at a working distance of up to 20 nm above the sample and the edges of particles often blur over tens of nanometers, such that a dry 30-nm cubic particle many appear to be 30 nm high but perhaps more than twice as wide.

The size and shape of an individual particle mounted on a substrate are also amenable to investigation by environmental transmission electron microscopy (ETEM). The groups of Martin and Buseck have used ETEM to observe liquid "shells" around a solid NaCl core between 72% and 76% RH.[7,8,15] Their ETEM studies primarily examined particles ~1 μm in width. In the same group, Wise *et al.* showed that NaCl nanocrystals with sides between 100 nm and 3 μm can exhibit reversible adsorption of layers of water up to almost 100 nm thick prior to deliquescence,[15] and onset of water uptake by dry NaCl particles was reported at all RH greater than 72%. As with SPFM, the apparent change in particle height measured by this technique is affected by both the polarizability and size of the sample.

The present study reports changes in the size and shape of NaCl nanocrystals as a function of RH as characterized by noncontact e-AFM. The e-AFM technique is sensitive primarily to changes in the size and shape of the particle, and only very weakly to changes in the chemical composition or dielectric constant. At values of RH several percentage points below the bulk deliquescence point of 75% at 23°C, the height of NaCl particles is found to increase by 2–5 nm. During the uptake of water a change in shape occurs in which the initially flat upper face of the particles becomes rounded. The observed changes in both height and shape are reversible and continuous, and are incompatible with an interpretation that posits a strong dependence of the measured height on the dielectric constant of the measured surface, as proposed by Miura *et al.* for a system that used noncontact AFM to study related salts.[29] The model presented below strongly suggests that the liquid layer consists of a concentrated ionic solution.

A model is presented for the height of the liquid layer on an NaCl particle as a function of RH. This model is based on measurements and models of adsorption of liquids onto insoluble substrates as originally observed by Derjaguin,[30,31] who used ellipsometry ("optical micropolarization") on quartz and glass substrates in the presence of water and other solvents in vapor to show that many of the vapors, including water, condensed and formed layers that were several nanometers thick. Models of these experiments due to Kuni[32,33] and Shchekin[34] included van der Waals forces—responsible for the initial adsorption of water—and an additional attractive force due to electrostatic layers on the presumably charged surface of the solid substrate. These models predicted that the thickness of the double layer would be approximately 2 nm, which is shorter than the Debye screening length expected from dissociation of ions at the solid-liquid interface (~10 nm), and near the Debye screening length of a 50 mM aqueous solution of monovalent ions.

II. EXPERIMENTAL

A. Substrate preparation

Silicon wafers (3 inches in diameter, 500 μm thick; University Wafers; South Boston, MA) were cut into pieces ~1 cm^2 in area, treated with UV-generated ozone plasma in a UV-oven (Bioforce Nanoscience; Ames, IA) for 30 minutes, immersed in a 1:500 (by mass) solution of octadecyltrichlorosilane (Gelest; Morrisville, PA) in chloroform for 3 hours, rinsed with chloroform, reoxidized for 5 minutes in the same UV-oven, and cleaned for 15 seconds with a jet of supercritical carbon dioxide. Oxidizing silane-treated substrates for 5 minutes prior to NaCl deposition caused the static contact angle with water to decrease from 109° on silicon freshly treated with silane to ~75°. This decrease in contact angle corresponds to a slight decrease in the surface free energy of the substrate regions, and helps to hold NaCl nanoparticles in place during AFM scans.

B. Deposition of NaCl aerosol

A solution of 0.1% Puratronic 99.999% pure NaCl with no anticaking additives (Alfa Aesar; Ward Hill, MA) in Milli-Q^{TM} purified water (Millipore; Billerica, MA) was chilled in an ice bath (~2°C), atomized at 20 psi by a flow of 95%/5% nitrogen/argon in a TSI model 9302 atomizer

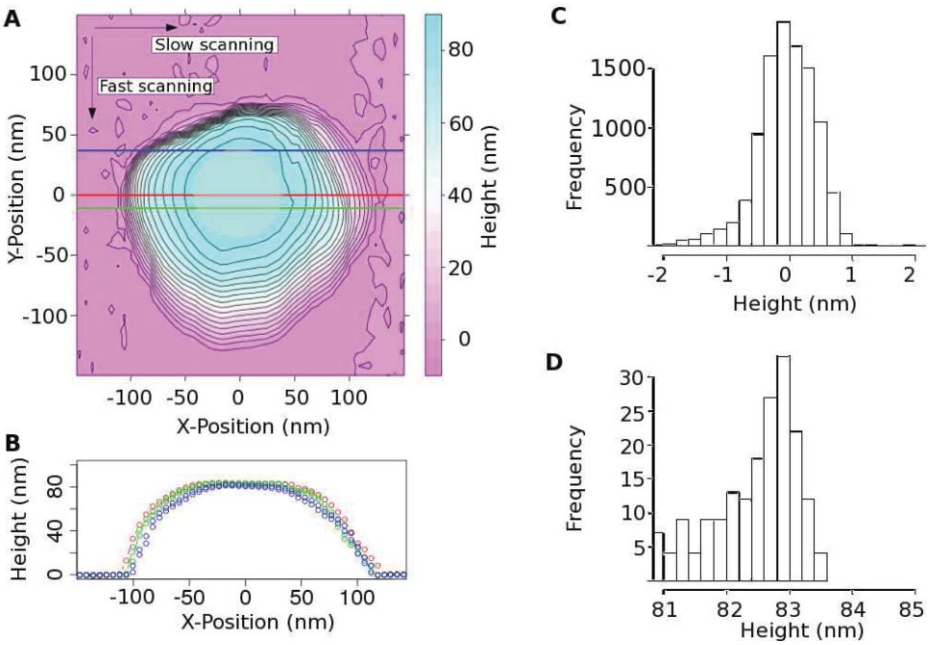

FIG. 1. Topography of a 83-nm (dry) wide NaCl particle at 52% RH after correcting for the tilt of the substrate (A). Contour plot of the particle. Contours are spaced by 5 nm. Also indicated are fast and slow scanning directions. The colored horizontal lines correspond to the points in (B). (B). Cross-sectional profiles of the NaCl particle shown in (A). (C). Histogram of the measured heights that correspond the the magenta region in (A). (D). Histogram of the measured heights that correspond to the gray circular region at the center of (A) (the "central region").

(TSI; Shoreview, MN), passed through a polycarbonate filter, (United Filtration Systems; Fraser, MI), passed through 30 cm of tubing heated to 40°C, slowed to a velocity of ~5 mm s^{-1} by adjusting a T-junction valve, and allowed to deposit onto a piece of treated silicon wafer in a glass chamber for 5 min to reach coverage of approximately 4 particles per μm^{-2} (greater particle densities complicated AFM imaging). A 1 g L^{-1} solution of NaCl was found to produce cubic crystals in a range of widths from ~30 nm to ~150 nm, with typical width near 100 nm. The experiments reported here were conducted only with the approximately cubic crystals generated using the 1 g L^{-1} solution.

C. Calibration and use of the e-AFM

The force of attraction between the sample and the AFM tip in non-contact mode can be approximated as directly proportional to ARd^{-2}, where d is the vertical working distance between the tip and the sample (5–10 nm), R the radius of curvature of the tip (10–20 nm), and A the Hamaker constant of the interaction between the tip and the sample (typically 1–10 kT).[35] The method for calibrating vertical distances measured by the noncontact AFM apparatus uses samples composed of a single material and implicitly assumes that the working distance, d, between the AFM tip and the sample is constant during the measurement. This assumption requires that a single value of the Hamaker constant characterize the entire surface of the calibration standard. Standards composed of a single material fit this assumption; real samples with one material, such as NaCl, deposited unevenly on a different substrate, such as silicon, do not strictly fit, but it can be shown from the dependence of the attractive force on the Hamaker constant and working distance that the distances maintained over different regions of the sample, d_{NaCl} and d_{Si}, do not differ by more than 2 nm as long as the Hamaker constants for those regions, A_{NaCl} and A_{Si}, do not differ by more than a factor of three. For measurements in air on nonmetallic condensed phases such as NaCl, Si, water, or NaCl solution, the Hamaker constants are unlikely to differ by more than 50%.[36] This work therefore assumes that only negligible error in height measurements is introduced by the differing Hamaker constants that characterize the interaction of the tip with different regions of the sample or substrate as RH changes.

All AFM data were acquired on a PicoPlus™ AFM (Agilent; Santa Clara, CA) using NSC15/AlBS silicon AFM probe tips (30° cone angle; MikroMasch; Sofia, Bulgaria) and PicoScan 5.0 software (Agilent, Santa Clara, CA). The AFM was calibrated in the x-, y-, and z-directions using known calibration standards (MikroMasch; Sofia, Bulgaria), and height measurements were estimated to be accurate to ±0.1 nm instrumental error. During a scan, the tip scans the particle from front to back in the fast direction, then moves one pixel along the slow direction [see Fig. 1(a)] and repeats this process until the particle is completely scanned. Acquiring each image requires 2–3 minutes. One such scan is shown in Fig. 1(a), with cross-sectional profiles shown in Fig. 1(b).

The RH of the AFM chamber was measured by a HIH-3610 humidity sensor (Honeywell; Freeport, IL) with a precision of ±0.5 percentage point and an accuracy of ±2 percentage points, calibrated at regular intervals against saturated solutions of NaCl, KCl, and KBr.[35,37] All experiments were performed at 23 ± 1°C.

The data for each particle were taken over a period of 3 hrs, during which the RH was varied cyclically: from an initial RH of 50%, followed by gradual increases of 1–2 percentage points until the RH reached 73% or higher, at which

time the RH was decreased to approximately 65%. The AFM chamber reached equilibrium at a new value of RH within 5–10 minutes of changing the setting. Each experiment included 3–4 of these cycles, although the final scans from some of the experiments were omitted if the particle appeared to have been modified by the tip.

An inherent limitation of AFM is that because the tip has finite curvature, it cannot accurately image features of a sample that have a radius of curvature less than that of the tip itself. In addition, after hours of use and occasional unintended contact with the sample, the radius of the curvature of the AFM tip may increase; images acquired with worn tips exhibit distortions at the sharp corners of the sample. In the experiments reported here, only new, unworn tips with radii of curvature 10–20 nm were used. Data obtained for the nearly flat central region of the top face of a cubic sample are unaffected by curvature of the tip; the height in this area can be measured to a precision of ∼0.1 nm, as noted above.

During an experiment, the resonant frequency of the AFM tip (and cantilever) was found to decrease with increasing RH, likely because of condensation of a minuscule amount of water onto the tip; as RH was restored the resonant frequency returned to its initial value. Other investigations have reported that an increase in RH from 30% to 80% reduced the resonant frequency of an AFM tip by 300–500 Hz.[38,39] Owing to the feedback loop that maintains a constant chosen set-point amplitude of oscillation of the tip, a decrease in the resonant frequency without retuning the chosen frequency of excitation would cause the tip to move away from the sample. This effect would eventually lead to a loss of topographical contrast (i.e., range of heights measured) in the AFM images as RH increases (decreasing RH leads to the reverse), and also to loss of any measurable interaction between the sample and the tip. The frequency of the driving voltage was therefore manually reduced by 50 Hz per 3 percentage points RH over 60% to compensate for the shift in resonant frequency.

Each experiment began with a chosen set-point amplitude of 2 V. Directly adjusting the driving voltage and set-point amplitude during the experiments allowed the instrument to maintain noncontact mode over the entire range of RH. The presence of at least several nanometers of topographical contrast indicated that the tip was sufficiently close to the surface, and the presence of no more than 0.05 V of phase contrast (in oscillations of the tip) indicated that the tip did not touch the surface or approach it too closely.[35,37] The PicoScan software provided both topographical contrast and phase-contrast in real time during scans.

D. Data analysis

The raw AFM data were extracted by the WSxM software package[40] (Nanotec; Madrid, Spain) for statistical analysis using R statistical software (http://r-project.org). Each pixel of raw data gives the height at one point of the sample relative to the height of the first point approached by the AFM at the beginning of the experiment. The effect of the tilt of the substrate and the approximately parabolic distortion in the position of the AFM tip in the fast direction (i.e., top to bottom of Fig. 1(a)) was accounted for by subtracting from all heights a paraboloidal fit of the substrate height. After such correction, the dataset yielded an array of height measurements that included a distribution of heights for the substrate floor (see Fig. 1(c)) and a distribution of heights for the nearly flat central region at the top of each NaCl particle (Fig. 1(d)). Dry particles were found to have flat tops (to within less than 0.5 nm) at 50% RH; a circle with diameter 90% of the height of the flat dry particle was used to bound the central region for which change in height was determined in subsequent measurements and higher RH [grey region in Fig. 1(a)]. At each RH, the height measurements of this central region was also fitted to a paraboloid, and the height of the vertex of the paraboloid relative to the substrate is reported as the height of the particle. The vertical error bars on each reported height for a given particle (Figs. 2 and 3) represent the standard error of the mean height of a known standard (±0.1 nm; see above), plus the standard errors of the two statistical fits: that of the substrate floor and the top of the particle, all added in quadrature (i.e., assuming independent errors). The horizontal error bars represent total uncertainty of ±2.1 percentage points in the measurement of RH, as reported by the manufacturer.

Because measurements of the dimensions of imaged particles are distorted by the finite dimensions of the AFM tips, the AFM method does not provide an accurate measure of changes in the volume of nanoscale samples. The changes in particle dimensions due to water uptake are reported here as changes in height, which for this technique is a more reliable measure of water uptake by the particles than are changes in volume. If the shape of the AFM tip were accurately known, it might be possible to remove some of the errors in shape due to these convolution effects; however, it is not possible to remove all such errors.[41] All data presented here resulted from studies of particles that produced AFM images at ∼50% RH consistent with approximately cubic profiles and sharply sloping (if not vertical) walls. Deconvolution according to Villarrubia's routines[41] reduced the distortion near the edges of the particles, but did not substantially change either the mean height of the central region or its standard error, as has been showed by numerous studies using scanning probe techniques.[42–44]

III. RESULTS

A. Noncontact AFM of dry salt crystals

A typical AFM scan of the height of a dry NaCl particle at 52% RH, rendered as a contour plot, is shown in Fig. 1(a). The AFM tip scanned the particle from the top to the bottom of the figure (the fast direction), line by line, followed by scrolling one pixel from left to right (the slow direction). Cross sections are shown in Fig. 1(b). This 83-nm high particle exhibited a flat central region approximately 75-nm wide, after correction for the tilt of the substrate. The height measurements of the central region of the particle were not adjusted separately from the correction for this tilt, so the result that the central region and the substrate are parallel emerges directly from the measurements.

The tilt of the cantilever relative to the substrate contributes to asymmetry in the slow direction of scanning.

Measurements taken along the x-direction in Figs. 1(a) and 1(b) exhibit a sharp increase in height as the tip moves from left to right onto the particle, but a comparatively gradual decrease in height as the tip moves off the particle. This asymmetry did not decrease with decreasing speed of scanning,

The bottom-to-top asymmetry as shown in Fig. 1(a) occurs because, at any given speed of scanning, the feedback loop in the instrument software adjusts the vertical position of the AFM tip more quickly to increases in the height of the sample than it does to decreases. Owing to the nonlinear force of interaction, approximated as $F \propto -d^{-2}$, an *increase* of tens of nanometers in the height of the sample as the tip moves onto a NaCl particle will lead to a *large* instantaneous increase in the interaction, whereas an identical *decrease* in the height as the tip moves off of the particle will cause only a *small* instantaneous decrease in the strength of the interaction.[35] In both cases, the feedback loop in the instrument adjusts the height of the scanner to compensate for the instantaneous change in the force of the interaction and maintain a constant vertical working distance. As a result, AFM scans show an *abrupt* increase in height at the leading edge of a particle [top of Fig. 1(a)] but a *gradual* decrease in height at the trailing edge [bottom of Fig. 1(a)]. Reducing the rate of the scan in the fast direction or reducing the gain of the instrument reduces the appearance of this asymmetry. Despite the asymmetry, the measured height of the central region of the particle [Fig. 1(d)] relative to the substrate on which it sits [Fig. 1(c)] does not change with increasing rate of scanning, because the distorted region is outside of the central region.

B. Deliquescence

A reversible increase in particle height (greater than 20-nm increase from the height at 50% RH for a ~90-nm particle) occurred near 75% RH at 23°C (Fig. 2). At RH above the DRH, particles grew irreversibly by several tens of nanometers in the 5–15 minutes required to complete two scans. Such rapid growth may have caused the tip to touch the liquid particle during a scan, and the possibility of contact—and therefore transfer of material—between the tip and a particle scanned at RH above the DRH cannot be excluded. Quantitative comparisons of particle height before and after such growth is not possible, and for this reason measurements taken after the images corresponding to point "18" on Fig. 2 are not shown.

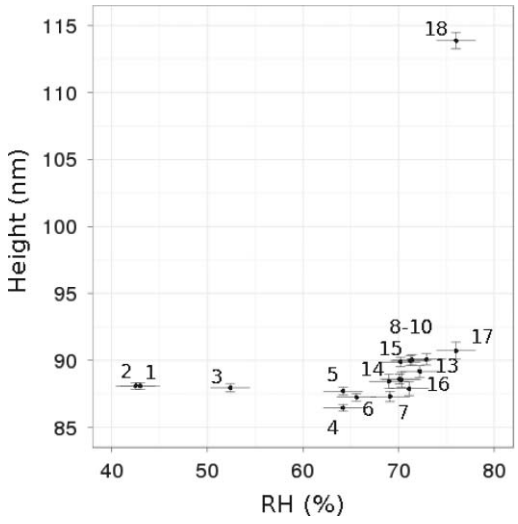

FIG. 2. Height of a 90-nm (dry) NaCl nanoparticle as a function of RH. Numbered data denote the order of measurement. Vertical uncertainties in represent the total standard error in the height of the plateau and of the substrate floor, and error due to instrumental noise added in quadrature. Horizontal uncertainties represent the uncertainties in the RH probe of ±2.1 percentage points.

As the RH increased from 65% to 74%, the particle in Fig. 2 appeared to undergo a gradual increase in height of approximately 3 nm. The order in which RH was varied suggests that this increase in height is reversible, and that this apparent uptake of water by NaCl at 65–75% RH is not deliquescence. Subsequent experiments in this study therefore focused on confirming and quantifying the hygroscopic behavior of NaCl nanoparticles at RH below the DRH.

C. Increase in height at RH below deliquescence

The heights of two typical particles relative to the supporting substrate as a function of RH are shown in Figs. 3(a) and 3(c). These data are representative of results from several identical experiments and were reproducible over the course of 3 hrs; the behavior of the samples did not appear to change when repeated measurements were conducted within 2–3 days of an initial experiment. At RH less than approximately 65% the height of one particle remained at or below 83 nm [Fig. 3(a)]. As RH increased above 65% the height of the particle began to increase, and at about 70% RH the increase became statistically significant; between 65% and 75% the height of the particle increased 5 ± 1 nm. During the 3-hr experiment, the measured height of the particle at a given RH did not depend on the past history of the particle, and the increase in particle height was found to be reversible. Reversible uptake of water by a 32-nm high NaCl particle also began between 65% and 75% RH [Fig. 3(c)]. The height of the 32-nm high particle increased by 3 ± 1 nm over the same range of RH.

The measurements shown in Figs. 3(b) and 3(d) give the heights measured across the central region of the particle—for example, the intersection of the red line and the gray circle in Fig. 1(a). By focusing on the central region, these measurements show that at 72–75% RH, the particles became noticeably rounded. This rounding was reversible between 70% and 75% RH, and was quantified by fitting cross-sectional height measurements taken in the central region of the particle along the slow scanning direction to a quadratic, where the radius of curvature, ρ, is evaluated at the vertex. These fits demonstrate that both an increase in height and greater rounding of the top surface are associated with the uptake of water, and ρ decreased from approximately 6 times the size of the particle near 60% RH to 1.5–2 times the particle size at 74% RH. Additionally, ρ appeared to increase with increasing particle size; at 74% RH, ρ for the 32-nm particle was approximately half that for the 83-nm particle.

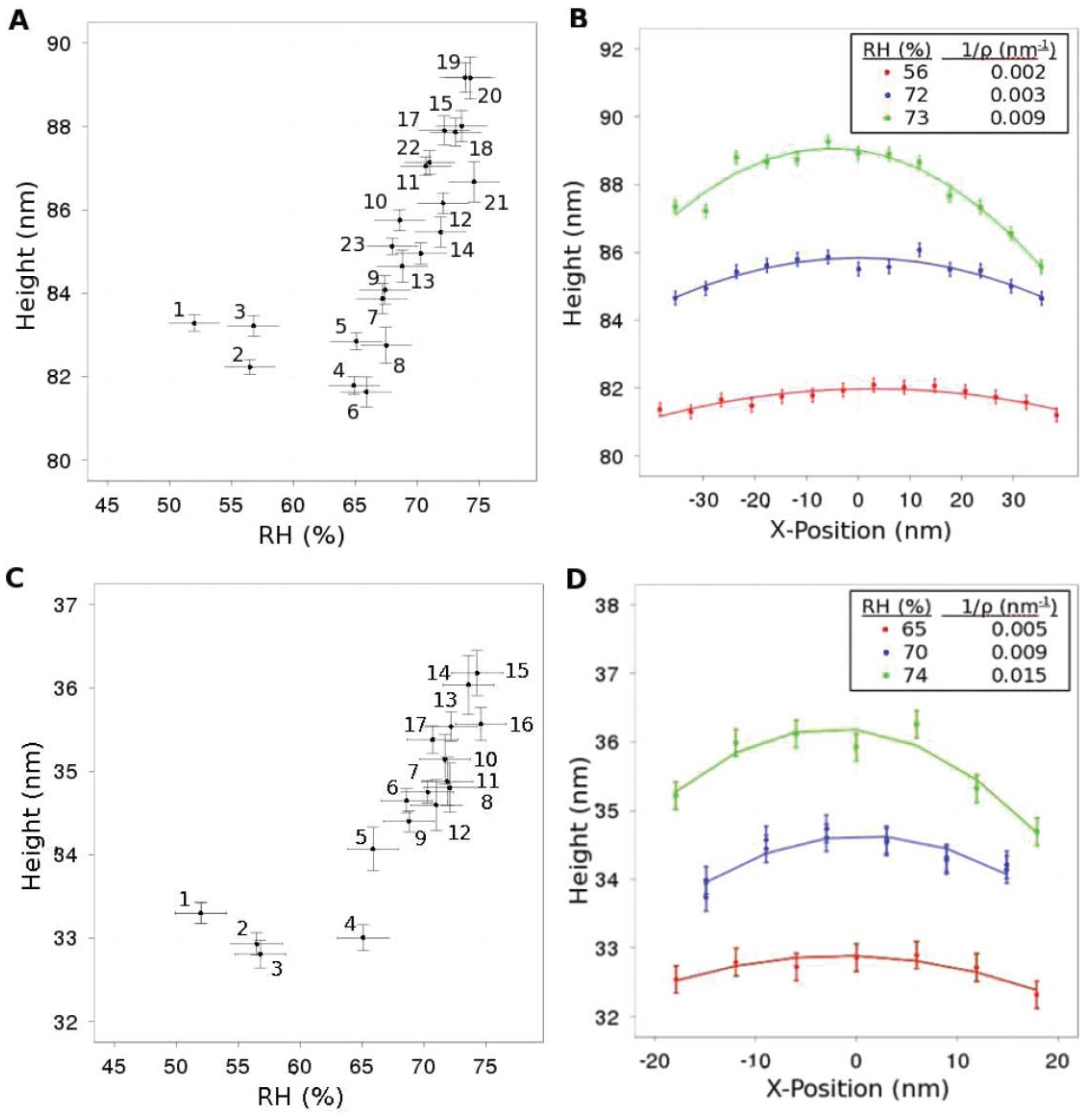

FIG. 3. NaCl nanoparticle height as a function of RH and position on crystal. (A). Height of a 83-nm (dry) NaCl nanoparticle as a function of RH, reported as the vertex of a parabaloid fit (see Fig. 1). (B). Height of the particle in (A) along a cross-section across the *x*-direction near the center of the particle at three values of RH [see blue line in Fig. 1(a)]. (C.) Height of a 32-nm (dry) NaCl nanoparticle as a function of RH. (D.) Height of the particle in (C) measured along a cross-section of the central region at different values of RH. Numbered data in (A) and (C) denote the order of measurement. Uncertainties in (A) and (C) are as in Fig. 2. Curves in (B) and (D) denote quadratic fits; ρ denotes the radius of curvature at the vertex of the curve. Uncertainties in (B) and (D) represent the standard error due to instrumental noise.

IV. Discussion

A. Surface contaminants

Volatile organic molecules are known to adsorb non-specifically onto samples except in ultra-high vacuum, and these contaminants may behave as surfactant coatings that affect the uptake of water on solid salts. The possibility of such contamination cannot be excluded in the present study; however, the reproducibility of height measurements suggests that only negligible contamination occurred over the course of each experiment, or alternatively that whatever contamination occurred was of negligible consequence. Additionally, previous work by Martin and others confirmed that deposition of aerosols by an atomizer did not result in samples that were more contaminated than samples generated by sublimation.[15]

B. Uptake of water

By using e-AFM to investigate the uptake of water by NaCl nanocrystals, we have shown that reversible adsorption of 2–5 nm of water occurs at lower RH than the abrupt, irreversible transition to the aqueous phase that constitutes deliquescence. Our data also indicate that either the layer of water is not of uniform thickness, and is instead thickest near the center of the particle face, or, alternatively, that the corners or edges of the crystal dissolve first, leading to the rounded shape. Distortions primarily due to convolution of the crystal edges with the AFM tip prevent exclusion of the latter possibility. The onset of measurable uptake of water appears to occur at RH as low as 65%, and the measured increase in height exceeds the uncertainty in measurements at 70% RH.

The interpretation of the present measurements assumes that all observed liquid layers at RH below DRH are NaCl-water solutions. Such solutions would normally be supersaturated, although the extent of supersaturation would be small at RH only a few percentage points below the DRH. Interestingly, the coexistence of phases observed below the DRH on these particles differs from the expected state of the macroscopic system evidently due to the presence of additional forces acting on the layer. Crystals over 10-nm in size are too large to be subject to Kelvin or curvature effects that can be detected by the current method at the RH values under consideration. A possible explanation for the observed behavior is that the steps, edges, or faces of the NaCl crystal may dissolve more readily than the bulk. In such situations, only a small fraction of the crystal mass, near the surface, is likely to be available for solvation, because steps and other irregularities do not persist deep into the solid. The e-AFM method used here cannot directly measure the composition of the layer, which must therefore be inferred through extension of bulk thermodynamic models into the thin-layer regime. Because changes in heights as measured are only a few nanometers, this discussion assumes that the total thickness of the liquid layer is indeed the change in height of the NaCl particle relative to the height measured at 50% RH.

The current results differ from the most closely related recent work on the uptake of water by NaCl surfaces in two respects. First, the present study demonstrated measurable changes in height at RH values less than those found in earlier investigations. In effect, the sensitivity of e-AFM to height differences of ~1 nm allowed elucidation of the transition from the several layers of water, as observed by Ewing,[5] Shindo,[45] and Cantrell,[4] to the liquid layers many nanometers in thickness observed by SPFM as employed by Salmeron's group[9,14,46] and ETEM as employed by Buseck, Martin, and colleagues.[7,8,15]

Second, the relative height change in particles at a given RH reported here is less by a factor of 2–4 than that reported earlier in studies using the SPFM or ETEM techniques. A possible explanation is that the non-contact e-AFM method relies on van der Waals interactions rather than electrostatic interactions, which are used by the SPFM and ETEM techniques. If the electrical properties of the sample do not change during such experiments, then SPFM and ETEM do effectively measure changes in height. If, however, ions do dissolve into the aqueous layers, then both the physical thickness and the electrical polarizability of the sample increase, and hence such techniques would overestimate the amount of water on the sample by confounding the effect of increasing polarizability with that of increasing height. In the present study by e-AFM, changes in the polarizability of the sample with changing RH affect the measurement only indirectly, through the Hamaker constant, which would be only negligibly affected as the air-particle interfaces changes with increasing RH from air-solid NaCl (at RH below 45%) to air-water as pure monolayers spread (between ~45% and ~60%) to air-solution near deliquescence.[36] The method of noncontact e-AFM is therefore particularly suited to characterization of changes of heights of particles whose phase or composition changes over the course of the experiment.

C. Modeling the uptake of water at RH below the bulk DRH

Important properties of the liquid layers observed at RH below the bulk DRH that must be accurately represented in a model are reversible formation, persistence at a given RH, and maximum height. Here a simple phenomenological thermodynamic model of formation of these layers is presented which incorporates the reversible work, $W_{total}(\ell)$, required to form a layer of thickness ℓ at a given value of RH. The model comprises three terms: the unfavorable bulk thermodynamics of forming a solution layer below the bulk DRH, $W_{cap}(\ell)$; favorable van der Waals forces between molecules of water vapor and the solid surface, $W_{vdW}(\ell)$; and an additional attractive term attributed to electrostatic interactions in the layer, $W_{exp}(\ell)$

$$W_{total}(\ell) = W_{cap}(\ell) + W_{vdW}(\ell) + W_{exp}(\ell). \quad (1)$$

The present data are incompatible with a model that omits the electrostatic term, even for a Hamaker constant of the interaction between the solid surface and water vapor, $A_{film} = 100kT$, which is far too large to be physically realistic. A derivation and discussion of each term follows below.

The layer is assumed to be infinitely thin and the capillary approximation is made wherein bulk properties are assigned to the material in the layer.[47] The Gibbs free energy of the vapor-particle system in the capillary approximation is

$$G_A = (N_1 - n_1)\mu_1^v + n_1\bar{\mu}_1^{sol} + n_2\bar{\mu}_2^{sol} + (N_2 - n_2)\bar{\mu}_2^c + \sigma_{cl}S + \sigma_{lv}S \quad (2)$$

where μ_1^v and $\bar{\mu}_1^{sol}$ are the chemical potentials for water in vapor and in solution, n_1 and n_2 are the number of molecules of water and NaCl ion-pairs in solution, respectively, and $\bar{\mu}_2^{sol}$ and $\bar{\mu}_2^c$ are the chemical potentials for salt in solution and in the crystalline phase, respectively. The surface tension at the crystal-liquid and liquid-vapor interfaces are given by σ_{cl} and σ_{lv}, and S gives the surface area of the respective interface. The total number of water molecules and NaCl ion pairs irrespective of phase are given by N_1 and N_2. In evaluation of differences in free energy terms $N_1\mu_1^v$ and $N_2\bar{\mu}_2^c$ cancel, leaving G_A in terms of contributions from the surface free energies of the two interfaces and the intervening solution, and an effectively constant term C

$$G_A = G_A(n_1, n_2) = n_1\left(\bar{\mu}_1^{sol} - \mu_1^v\right) + n_2\left(\bar{\mu}_2^{sol} - \bar{\mu}_2^c\right) + \sigma_{cl}S + \sigma_{lv}S + C \quad (3)$$

where $C = N_1\mu_1^v + N_2\bar{\mu}_2^c$ depends only on temperature, RH, and the quantities of water and NaCl in the system.

It is assumed that near the measured bulk DRH, 75%, a liquid layer of solution is always present. Free energies will be computed relative to the thin-layer reference state, defined as

$$G_{TL} \equiv G_A(0, 0) = \sigma_{cl}S + \sigma_{lv}S + C \quad (4)$$

for which n_1 and n_2 are negligibly small ($\ell = 0$), and the interfaces remain intact, but are assigned zero thickness consistent with the capillarity approximation. The solution-thermodynamic contribution to the reversible work required

to create a layer thicker than the thin liquid layer of the reference state is therefore defined at any specified value of RH by

$$W_{cap}(n_1, n_2) = G_A(n_1, n_2) - G_{TL} = n_1\left(\bar{\mu}_1^{sol} - \mu_1^{v}\right) + n_2\left(\bar{\mu}_2^{sol} - \bar{\mu}_2^{c}\right). \quad (5)$$

The first term on the right-hand side of Eq. (5) vanishes because $\bar{\mu}_1^{sol} = \mu_1^{v}$ for water vapor in equilibrium with the solution layer across a flat surface. The second term vanishes only at the bulk DRH, under which condition water vapor is in equilibrium with NaCl solution and $\bar{\mu}_2^{sol} = \bar{\mu}_2^{c}$. Thus, at the bulk DRH, $W_{cap} = 0$ and no work is required to form the layer, but at any RH $<$ DRH$_{bulk}$, positive work is required.

For an ideal solution obeying Raoult's law, $x_1 = RH/100$, where x_1 is the mole fraction of water in the solution layer, and $x_2 = 1 - x_1$ is the mole fraction of NaCl. Equation (5) simplifies to

$$W_{cap}(n_1, n_2) = n_2\left(\bar{\mu}_2^{sol} - \bar{\mu}_2^{c}\right) = n_2 kT \ln\left(\frac{x_2}{\bar{x}_2}\right). \quad (6)$$

For a nonideal solution the mole fraction ratio should be replaced by the solute activity as described below. The mole fraction of NaCl in a bulk-saturated solution, $\bar{x}_2 = 0.25$ corresponds to $\bar{x}_1 = 0.75$ at $DRH = 75\%$. For any $RH < DRH$, $x_2 > \bar{x}_2$, so the logarithm is positive and forming the layer requires expending work.

Each NaCl ion pair brings n_1/n_2 molecules of water to the layer, so the total volume of the layer is given by

$$V = \ell S = (n_1 v_1 + n_2 v_2) \quad (7)$$

where v_1 and v_2 are the molecular volumes of water and salt in the layer. Combining Eqs. (6) and (7) yields $\tilde{W}_{cap}(\ell)$, the work, per unit area, required to form a layer of thickness ℓ, as

$$\tilde{W}_{cap}(\ell) = \ell \frac{kT \ln\left(\frac{x_2}{\bar{x}_2}\right)}{\left(v_2 + \left(\frac{n_1}{n_2}\right) v_1\right)} = \ell \times \alpha_{RH}. \quad (8)$$

The fraction in Eq. (8), abbreviated as α_{RH}, is easily evaluated as a function of RH for values of v_1 and v_2 characteristic of the salt. For a real solution, the activity of the salt replaces the mole fraction ratio. The activities and partial molar volumes (as functions of mole fractions) must be used and can be estimated from thermodynamic data of water uptake, such as reported by Tang,[12] using Gibbs-Duhem integration.[48] Activities obtained from the Tang measurements were used in the fits presented below.

The energetically favorable contribution to the formation of a liquid layer due to van der Waals interactions between liquid and solid is conveniently expressed in terms of the force, per unit area, required to separate the bounding solid and vapor phases,

$$\Pi(\ell) = -\frac{dP(\ell)}{d\ell} = \frac{A_{film}}{6\pi\ell^3}, \quad (9)$$

where A_{film} is the Hamaker constant (typically between $1kT$ and $10kT$ for two nonconducting condensed phases interacting across air[36]) and $P(\ell)$ gives the surface free energy, per unit area. Integration over ℓ gives the energetic contribution by van der Waals forces,

$$\tilde{W}_{vdW}(\ell) = \frac{A_{film}}{12\pi\ell^2}. \quad (10)$$

A phenomenological contribution to the energy of formation of liquid layers on insoluble nuclei proposed by Widom,[32] Kuni,[33] and others[34] is

$$\tilde{W}_{exp}(\ell) = K\xi exp\left(\frac{-\ell}{\xi}\right). \quad (11)$$

According to these investigators, an electrical double layer exists at the solid-liquid interface, with a characteristic length, ξ, on the order of the Debye screening length. Widom noted that the parameter ξ characterizing the uptake of polar solvents onto solid particles can be 10 times the radius of solvent molecules.[32] Kuni *et al.* suggested that both the prefactor K and the length-scale ξ must be empirically determined.[33] Shchekin *et al.*[34] broadened this model to treat soluble nuclei, but they did not equate ξ with the Debye screening length. The obvious difficulty with invoking electrostatic interactions in a system with solvated ions is that the Debye length in saturated NaCl solution is about 0.1 nm, or only about one third the diameter of a water molecule. Thus, any charged surface coated with saturated NaCl would be completely screened by soluble ions within the first few layers of solution, and electrostatic effects would not extend over a distance comparable to the thickness of the liquid layers observed in the present work. The discussion below therefore attempts to complete a purely phenomenological model of uptake of water on NaCl nanoparticles by including the exponential term (Eq. (11)) in the expression for the total free energy of the liquid layer.

Because a crystal of NaCl with adsorbed water is known to be positively charged at the solid-liquid interface,[49] the prefactor K in Eq. (11) for the formation of liquid layers on a charged surface can be calculated according to the formula used by Bergeron,[50] Hunter,[51] and Israelachvili[36] as $64kTn_0$, where n_0 is the number density of ions per unit volume in the liquid layer. For a saturated solution of NaCl on a sparsely charged surface, this formula gives a value for K of approximately $1.5 \times 10^9 kT$ cm^{-3}, the value also used by Kuni *et al.*,[33] whereas Shchekin *et al.*[34] used $1 \times 10^8 kT$ cm^{-3}. Noting that none of these attempts at justification is free of difficulty, we simply regard Eq. (11) as an empirical relation that, when added to the right-hand sides of Eqs. (8) and (10), yields an expression for the total free energy per unit area for formation of the liquid layer

$$\tilde{W}_{total}(\ell) = \tilde{W}_{cap}(\ell) + \tilde{W}_{vdW}(\ell) + \tilde{W}_{exp}(\ell) = \alpha_{RH} \times \ell + \frac{A_{film}}{12\pi\ell^2} + K\xi exp\left(-\frac{\ell}{\xi}\right) \quad (12)$$

where K and ξ are treated as adjustable parameters. The best fit of the 83-nm particle data occurred with $\xi \simeq 2$ nm, $K \simeq 2 \times 10^8\, kT$ cm^{-3} and $A_{film} \simeq 1\, kT$ (Fig. 4). The thicknesses of the observed layers are too large to be consistent

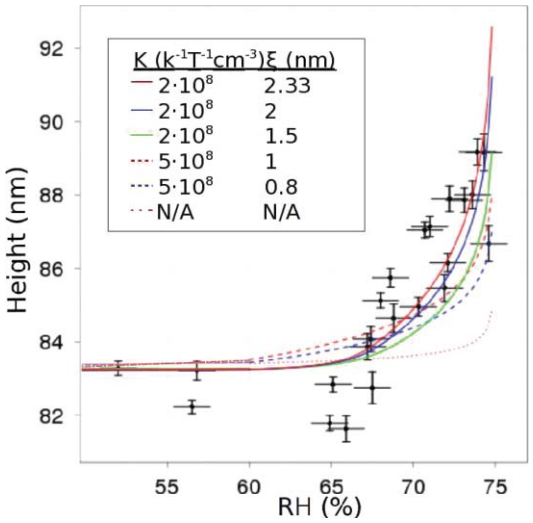

FIG. 4. Measured heights (circles) as a function of RH for the 83-nm (dry) nanoparticle shown in Fig. 1(A), and calculated heights (lines) obtained by adding 83 nm to the thickness of a liquid layer formed according to Eq. (12) without the electrostatic attraction (i.e., $K = 0$; dotted red line; $A_{film} = 1kT$) or with electrostatic term (all others; $A_{film} = 10kT$). N/A means the exponential term has been omitted.

with a screening length of 1 nm, which is ten times the Debye length for saturated NaCl solution. This finding echoes work by Derjaguin and Zorin, who observed that adsorption of water, alcohols, fatty acids, and alkanes onto insoluble substrates formed layers several nanometers thick.[30,31] The thickness of the layers examined in those studies did not appear to correlate with the Debye length of the systems, and this observation may have led to Kuni's claim that both the prefactor K and characteristic length ξ must be determined empirically.[33] In their model of a layer forming on a soluble salt crystal, Shchekin *et al.*[34] used a value for ξ of 2.33 nm, corresponding neither to the Debye length of pure water ($\sim$1 μm) nor to that of a solution with greater than a 1 mM concentration of ions ($\sim$1 nm at 100 mM).

The thermodynamics at the solid-liquid interface requires that the liquid layer contain ions. In addition, the results from the Salmeron group[9] are further evidence of highly polarizable liquid layers—that is, of NaCl solutions rather than pure water. The assumption of a characteristic length on the nanometer scale leads to a much better fit of the present data than the assumption of electrostatic effects persisting only over the Debye length. The model does not, however address the apparent size-dependence of the thickness and curvature of the liquid-layer.

V. CONCLUSIONS

Studies by noncontact environmental AFM revealed reversible growth of up to 5 nm thick liquid layers on substrate-supported NaCl nanoparticles and a rounding of the upper surface of particles at RH below the DRH. An observed increase in the curvature at the top surface of the particle with increasing RH suggests that some NaCl dissolves at the surface between 65% and 75% RH, and a model is presented that accounts for this result. The observed thickness is a factor of 2–4 less than those reported by other scanning probe studies that measured surface polarizability of NaCl; a possible explanation for this difference is the presence of dissolved ions in the layer, which would increase the SPFM or ETEM signal relative to a pure water layer, but which would have negligible effect on the topography as measured by e-AFM. The e-AFM method is sensitive enough to detect liquid layers 2-nm thick on NaCl surfaces at RH as low as 70%. The lateral dimensions of aerosol particles in the atmosphere may therefore be as much as 10 nm greater at RH slightly below the DRH than when at much lower RH. This increase in thickness due to the presence of a liquid layer represents a previously undetected site for atmospheric reactions in the aqueous phase, but seems unlikely to have much impact on light scattering by such particles.

ACKNOWLEDGMENTS

This work was supported by the Laboratory Directed Research and Development Program at Brookhaven National Laboratory under Contract No. DE-AC02-98CH10886 of the U.S. Department of Energy. We thank Susan Oatis of Stony Brook University for advice on the synthesis apparatus, and Hendrik Hansen-Goos and J. D. Wettlaufer of Yale University for helpful discussions.

[1] J. W. Gibbs, *The Scientific Papers of J. Willard Gibbs, Vol. 1: Thermodynamics* (Dover, New York, 1961).
[2] E. Woods III, C. N. Wivagg, and D. Chung, J. Phys. Chem. A **111**, 3336 (2007).
[3] S. Dietrich and M. Schick, Phys. Rev. B **33**, 4952 (1986).
[4] W. Cantrell, C. McCrory, and G. E. Ewing, J. Chem. Phys. **116**, 2116 (2002).
[5] G. E. Ewing, Struct. Bond. **116**, 1 (2005).
[6] M. Ebert, M. Inerle-Hof, and S. Weinbruch, Atmos. Environ. **36**, 5909 (2002).
[7] T. A. Semeniuk, M. E. Wise, S. T. Martin, L. M. Russell, and P. R. Buseck, Atmos. Environ. **41**, 6225 (2007).
[8] M. E. Wise, T. A. Semeniuk, R. Bruintjes, S. T. Martin, L. M. Russell, and P. R. Buseck, J. Geophys. Res. **112**, D10224 (2007).
[9] K. Arima, P. Jiang, D.-S. Lin, A. Verdaguer, and M. Salmeron, J. Phys. Chem. A **113**, 9715 (2009).
[10] I. N. Tang and H. R. Munkelwitz, J. Appl. Meteorol. **33**, 791 (1994).
[11] I. N. Tang, A. C. Tridico, and K. H. Fung, J. Geophys. Res. **102**, 23269 (1997).
[12] I. N. Tang, J. Geophys. Res. **102**, 1883 (1997).
[13] Q. Dai, J. Hu, and M. Salmeron, J. Phys. Chem. B **101**, 1994 (1997).
[14] A. Verdaguer, G. M. Sacha, D. F. Ogletree, and M. Salmeron, J. Chem. Phys. **123**, 124703 (2005).
[15] M. E. Wise, S. T. Martin, L. M. Russell, and P. R. Buseck, Aerosol Sci. Technol. **42**, 281 (2008).
[16] A. S. Wexler and J. H. Seinfeld, Atmos. Environ. **25A**, 2731 (1991).
[17] I. N. Tang and R. H. Munkelwitz, Atmos. Environ. **27A**, 467 (1993).
[18] D. J. Cziczo and J. P. D. Abbatt, J. Phys. Chem. A **104**, 2038 (2000).
[19] M. J. Rossi, Chem. Rev. **103**, 4823 (2003).
[20] W. R. Simpson, R. von Glasgow, K. Riedel, P. Anderson, P. Ariya, J. Bottenhein, J. Burrows, L. J. Carpenter, U. Friess, M. E. Goodsite, D. Heard, M. Hutterli, H.-W. Jacobi, L. Kaleschke, B. Neff, J. Plane, U. Platt, A. Richter, H. Roscoe, R. Sander, P. Shepson, J. Sodeau, A. Steffen, T. Wagner, and E. Wolff, Atmos. Chem. Phys. **7**, 4375 (2007).
[21] J. Arsic, D. M. Kaminski, N. Radenovic, P. Poodt, W. S. Graswinckel, H. M. Cuppen, and E. Vlieg, J. Chem. Phys. **120**, 9720 (2004).
[22] S. J. Peters and G. E. Ewing, Phys. Chem. B **101**, 10880 (1997).
[23] J. C. Schlenker, A. Malinowski, S. T. Martin, H.-M. Hung, and Y. Rudich, J. Phys. Chem. A **108**, 9375 (2004).
[24] T. Rosenoern, J. C. Schlenker, and S. T. Martin, J. Phys. Chem. A **112**, 2378 (2008).

[25]G. Biskos, A. Malinowski, L. M. Russell, P. R. Buseck, and S. T. Martin, Aerosol Sci. Technol. **40**, 97 (2006).
[26]S. Romakkaneimi, K. Hameri, M. Vakeva, and A. Laaksonen, J. Phys. Chem. A **105**, 8183 (2001).
[27]A. L. Mifflin, M. L. Smith, and S. T. Martin, Phys. Chem. Chem. Phys. **11**, 10095 (2009).
[28]L. Greenspan, J. Res. Nat. Bureau Standards A Phys. Chem. **81**A(1) (1977).
[29]K. Miura, T. Yamada, M. Ishikawa, and S. Okita, Surf. Sci. **140**, 415 (1999).
[30]B. V. Derjaguin and Z. M. Zorin, Zhourn. Fiz. Khimii **29**, 1010 (1955).
[31]B. V. Derjaguin and Z. M. Zorin, Zhourn. Fiz. Khimii **29**, 1755 (1955).
[32]F. M. Kuni, A. K. Shchekin, A. I. Rusanov, and B. Widom, Adv. Colloid Interface Sci. **95**, 71 (1996).
[33]F. M. Kuni, A. K. Shchekin, and A. P. Grinin, Phys. Usp. **44**, 331 (2001).
[34]A. K. Shchekin, I. V. Shabaev, and A. I. Rusanov, J. Chem. Phys. **129**, 214111 (2008).
[35]A. Checco, Y. Cai, O. Gang, and B. M. Ocko, Ultramicroscopy **106**, 703 (2006).
[36]J. N. Israelachvili, *Intermolecular and Surface Forces with Applications to Colloid and Biological Systems* (Academic Press, Orlando, 1985).
[37]A. Checco and B. M. Ocko, Phys. Rev. E **77**, 061601 (2008).
[38]T. Thundat, R. J. Warmack, and G. Y. Chen, Appl. Phys. Lett. **64**, 2894 (1994).
[39]H. Sone, Y. Fujinuma, T. Hieida, and S. Hosaka, SICE Ann. Conf. in Fukui, 2121 (2003).
[40]I. Horcas, R. Fernandez, J. M. Gomez-Rodriguez, J. Colchero, J. Gomez-Herrero, and A. M. Baro, Rev. Sci. Instrum. **78**, 013705 (2007).
[41]J. S. Villarrubia, J. Res. Nat. Inst. Standards Technol. **102**, 425 (1997).
[42]S. Du, L. Cai, and D. Gao, IEEE Trans. Instrum. Meas. **55**(2), 507 (2006).
[43]Y. Harada, H. Sone, and S. Hosaka, Japan. J. Appl. Phys. **47**, 6186 (2008).
[44]F. Marinello, P. Bariani, S. Carmignato, and E. Savio, Measurement Sci. Technol. **20**, 084013 (2009).
[45]H. Shindo, M. Ohashi, O. Tateishi, and A. Seo, J. Chem. Soc. Faraday Trans. **93**, 1169 (1997).
[46]J. Hu, X.-D. Xiao, and M. Salmeron, Appl. Phys. Lett. **67**, 476 (1995).
[47]P.-G. de Gennes, F. Brochard-Wyart, and D. Quere, *Capillarity and Wetting Phenomena: Drops, Bubbles Pearls Waves* (Springer, Paris, 2004).
[48]G. N. Lewis and M. Randall, *Thermodynamics* (McGraw-Hill, New York, 1961).
[49]P. Cabrera-Sanfelix, D. Sanchez Portal, A. Verdaguer, G. R. Darling, M. Salmeron, and A. Arnau, J. Phys. Chem. C **111**, 8000 (2007).
[50]V. Bergeron, J. Phys.: Condens. Matter **11**, R215 (1999).
[51]R. J. Hunter, *Foundations of Colloid Science* (Clarendon Press, Oxford, 1987), Vol. 1.